

# INTEGRATING CONTINUOUS POLLUTANT MEASUREMENTS WITH TIME-LAPSE PHOTOGRAPHY TO EVALUATE INLAND VESSEL SURROUNDINGS' INFLUENCE ON WHEELHOUSE INDOOR AIR QUALITY

## OLIVIER SCHALM

Antwerp Maritime Academy, Noordkasteel-Oost 6, 2030 Antwerp, Belgium  
e-mail: olivier.schalm@hzs.be (Author for correspondence)

## WERNER JACOBS

Antwerp Maritime Academy, Noordkasteel-Oost 6, 2030 Antwerp, Belgium  
e-mail: werner.jacobs@hzs.be

## ACKNOWLEDGMENTS

The authors thank Flanders Innovation & Entrepreneurship (VLAIO) for the financial support of the TETRA-project ELGAS (project number HBC.2019.2033). The authors also thank Joeri Verbiest and Lorenz Adriaensen of Karel de Grote University of Applied Sciences and Arts for their contribution in the air quality monitoring campaign. The authors also thank Steve Vanlanduit for performing the time-lapse measuring campaign.

## Keywords

Inland ship, indoor air quality, surroundings, causal network

**Thematic area:** Sea pollution and environmental protection

## Abstract

The indoor air quality in the wheelhouse of an inland tanker was assessed through monitoring campaigns. The continuous-time measurements gathered data on NO<sub>2</sub>, O<sub>3</sub>, NO, CO, total volatile organic compounds (TVOC), and particulate matter (PM<sub>2.5</sub>). The time series exhibited irregular concentration profiles characterized by narrow and broader peaks atop a gradually fluctuating baseline. These peaks denote sudden environmental changes, occurring within specific time frames and locations, indicating moments of poorer indoor air quality. The synchrony between peaks of different pollutants suggests that many of the narrow pollution peaks originate from exhaust emissions. Previous research has indicated that exhaust gas in outdoor air could infiltrate the wheelhouse via the ventilation system. However, multiple factors within the ship's vicinity (e.g., nearby industries, specific manoeuvres, or passing vessels) could also contribute to the occurrence of pollution peaks in the wheelhouse. To explore the synchrony between pollution peaks in the wheelhouse and events in the surroundings of the ship, a time-lapse camera capturing time-stamped images of the ship's front view has been installed. Analysis of these images in conjunction with the simultaneous occurrence of pollution peaks as observed in time series indicates the existence of multiple pollution sources influencing the indoor air quality in the wheelhouse. The various sources of pollution form an interlinked network of hazards that collectively influence indoor air quality. Each source has the potential to induce changes within this network and can, to a certain extent, affect other hazards. Furthermore, non-polluting elements within this network also contribute significantly to the variable behaviour of the network. For example, crew decisions regarding navigation and manoeuvres play affect the dynamics of this network.

## 1 INTRODUCTION

Sensor-based monitoring campaigns measuring air quality within the enclosed environment of inland ship wheelhouses provide a wealth of information [1,2]. They give an insight what pollutants a ship emits [3–9] and how they infiltrate in the wheelhouse [10,11]. However, the absence of explicit event labels poses a significant obstacle to understanding the underlying drivers of pollution dynamics. Besides the ship's own exhaust fumes, emissions from all other ships in the surroundings [12], poorer air quality in which ships operate such as harbours [13], nearby industrial activities, or ship operations could impact the indoor air quality as well [14–16]. One way to assess the impact of the ship itself on the indoor air quality is to monitor the ship's changes in motion and orientation and check their synchrony with the occurrence of pollution peaks. GPS information also provides some insight into the ship's surroundings, such as whether it is navigating through industrial or rural areas, passing a bridge, or located at a lock. However, there are many other events that remain unseen. Therefore, relying solely on motion and GPS data may not capture the full range of factors influencing air quality. To gain deeper insight in the occurrence of events in the vicinity of the ships, a time-lapse camera has been installed that captures photos of the ship's front view during the air quality monitoring campaign. The timestamped photos have been used to identify events such as waiting next to another ship in a lock or performing specific operations such as bunkering a merchant ship.

The indoor air quality in the wheelhouse of an inland tanker has been assessed through monitoring campaigns. The continuous-time measurements gathered data on NO<sub>2</sub>, O<sub>3</sub>, NO, CO, total volatile organic compounds (TVOC), particulate matter (PM<sub>2.5</sub>) and GPS while the time lapse camera took photos of the ship's front view. This study aims to elucidate the interplay between pollution events and occurrences in the vicinity of the ship, thereby offering valuable insights into the broader dynamics at play.

## 2 BACKGROUND

An outlier, in statistical terms, refers to a data point that significantly deviates from other observations in a dataset, implying a different underlying condition or measurement error [17–19]. In the context of air quality monitoring campaigns conducted within the enclosed environment of inland ship wheelhouses, complex and dynamic patterns in measured environmental parameters have been revealed. These patterns often include outliers, where certain data points deviate substantially from the rest of the dataset. These outliers manifest as diverse short-term features, such as isolated peaks of varying widths, series of overlapping peaks, or valleys superimposed on a slowly fluctuating baseline. Moments of heightened pollutant concentrations are particularly significant as they can impact the health of the crew, even when air quality meets legislative standards. These features are identified when a subset of consecutive data points exhibits distinct properties that set them apart from neighboring data points, often marked by a significant increase or decrease in signal relative to the baseline.

Outliers, including peaks and valleys, typically arise due to processes different from those affecting the rest of the data. These processes are often linked to events occurring in or around the ship. For instance, emitted exhaust gas tends to accumulate around the ship when the relative wind speed and direction align closely with the ship's speed and direction. A deeper understanding of such events could be instrumental in improving air quality within wheelhouses. However, while environmental monitoring campaigns offer insights into temporal trends, they often lack detailed information to fully explain the events driving these patterns. The limited causal information available in the time series often comprises signature patterns, such as the synchrony of outliers observed across different parameter time series, which can indicate specific sources. For example, simultaneous peaks of temperature, relative humidity, and CO<sub>2</sub> levels may indicate human presence in the wheelhouse, while concurrent peaks of NO and NO<sub>2</sub> suggest the entry of exhaust gas emissions through the ventilation system.

The term 'outlier' is commonly used in data analysis. It represents sudden occurrences that take place in the data world and offer descriptions of what is happening (see data world in Fig. 1). 'Events' denote sudden occurrences that take place in the real world (see real world in Fig. 1). They provide insight into the reasons why something is happening. This contribution aims to investigate the relationship between outliers identified in air quality data and the events taking place in and around the ship as identified with time-lapse photography.

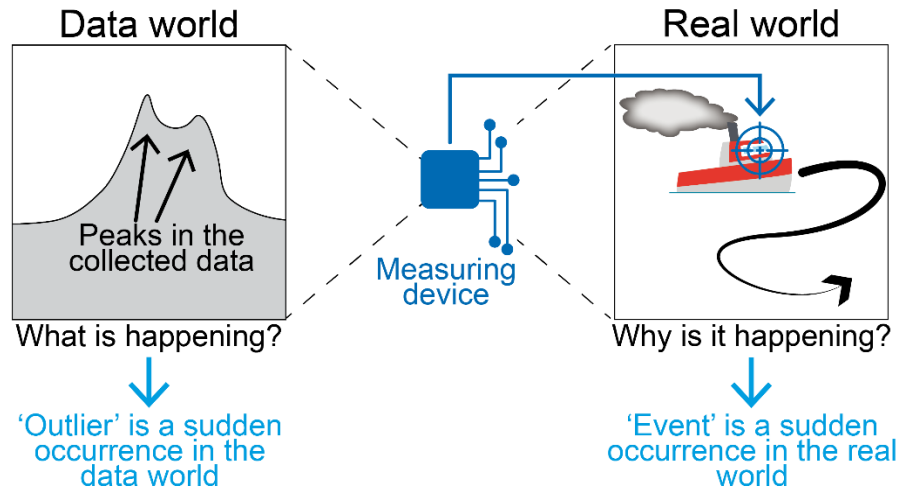


Fig. 1: Schematic representation of the difference between outlier and event and how they are related.

## 2 EXPERIMENTAL

### 2.1. Measuring campaign

During the measuring campaign from 26 January to 1 February 18 March 2021, an in-house developed sensor box to measure various environmental parameters has been installed in the wheelhouse of an inland tanker dedicated to the bunkering of merchant ships. The sensor box has been described elsewhere and is able to monitor temperature, relative humidity, CO<sub>2</sub>, PM<sub>1</sub>, PM<sub>2.5</sub>, PM<sub>10</sub>, CO, NO<sub>2</sub>, O<sub>3</sub>, NO, H<sub>2</sub>S, SO<sub>2</sub>, and TVOC [1]. Sensors do not generate signals as reliable as state-of-the-art reference instruments, but they are good enough to assess air quality [20,21]. The concentrations of H<sub>2</sub>S and SO<sub>2</sub> [22] are close or below the detection of the sensors (< 5 ppb) and will be omitted in this study. The sensor box is also able to measure GPS signals. All parameters are measured with a sampling time of 3 minutes. The monitoring campaign results in a data matrix with measurements arranged in rows and parameters arranged in columns. The first column entails the timestamp. The collected data matrix contains 2823 rows/measurements.

The installation of a time-lapse camera on the front window using a suction cup mount allowed the continuous visual record during the air quality monitoring campaign. This resulted in a dataset of 7,807 photos, each taken at one-minute intervals. The organization of this dataset is meticulously structured, with each photo's filename embedding the timestamp of its capture. This naming convention facilitates a seamless chronological analysis of the data collected, enabling an intricate visual timeline that complements the air quality measurements.

### 2.2. Data processing of the air quality data

The collected air quality data undergoes a preprocessing stage as the first step in its analysis. This data preparation phase comprises several steps: inserting missing rows, filling absent data via linear interpolation, identifying erroneous data and replacing them through linear interpolation, correcting inconsistencies by replacing values outside an acceptable range with interpolated estimates, and smoothing out noise. Microsoft Excel is employed to both introduce missing rows and bridge gaps in data through linear interpolation. Then, noise has been suppressed by applying a central moving average using a span of 5 data points.

A variety of methods exists to identify outliers. However, there is no universal recipe and the data analyst must choose the right approach [23]. Due to a lack of prior information about the characteristics of the data and the type of outliers, outlier detection has been done manually. However, it should be possible to perform this task using an algorithm [4]. For the manual peak identification, the time series data are graphically represented to facilitate visual identification of peaks. Overlapping peaks characterized by several local maxima are considered a single entity to maintain clarity in the analysis. For every identified peak or series of overlapping peaks with several local maxima, the corresponding

data points in the matrix are marked in red, and the maximum of the outlier is emphasized in bold. After the identification of an outlier, a comprehensive summary is compiled in a new matrix, detailing the start and end timestamps of each outlier, the timestamp of the maximum value, the type of pollutant involved, the outlier's maximum value, the corresponding z-score, and the GPS coordinates at which the maximum value occurred. A similar approach is employed for identifying valleys, with the primary difference being the focus shifted towards the minimum value of the outlier. Through this approach as visualized in Fig. 2a, peaks within the time series are meticulously described by a fixed series of features arranged in a matrix format. These features are:

- **Timestamp Start Outlier:** This moment marks the initial moment when a deviation from the baseline is noticed. Identifying this point can be challenging, especially if the deviation (peak or valley) develops gradually over time, making it less distinct;
- **Timestamp Maximum or Minimum Value of the Outlier:** This timestamp precisely identifies when an outlier reaches its highest value (peak) or lowest value (valley) within the observed range. It marks the moment of maximum deviation from the baseline. In cases where multiple moments share the same maximum value, the first data point is selected;
- **Timestamp End Outlier:** This timestamp indicates when the data returns to values similar to the baseline, signifying the end of the outlier. The data points within the start and end timestamps of the outlier in the data matrix are highlighted in red;
- **Duration:** Represents the total time expressed in minutes from the start to the end of the outlier. This metric quantifies the length of the deviation period;
- **Parameter:** Refers to the specific environmental parameter (e.g., PM<sub>2.5</sub>, NO<sub>2</sub> levels) for which a deviation (peak or valley) is observed;
- **Shape:** Describes the overall appearance of the outlier in the time series data. It can be a single peak or valley with one maximum or minimum point, or a complex pattern featuring a series of overlapping peaks or valleys;
- **Maximum or Minimum Value in the Range:** The highest (for peaks) or lowest (for valleys) recorded value of the outlier, as measured by one of the monitoring sensors during the outlier.
- **Corresponding Z-Score of the Minimum or Maximum Value:** The Z-score associated with the peak or valley value, indicating how many standard deviations a peak maximum or valley minimum deviates from the mean. This statistic helps assess the outlier's intensity relative to the normal data distribution.
- **GPS Latitude of the Maximum/Minimum Value:** The geographical latitude where the maximum or minimum value was recorded, providing spatial context to the outlier outlier.
- **GPS Longitude of the Maximum/Minimum Value:** Similarly, this is the geographical longitude where the peak or valley occurred, further pinpointing the location of the deviation.

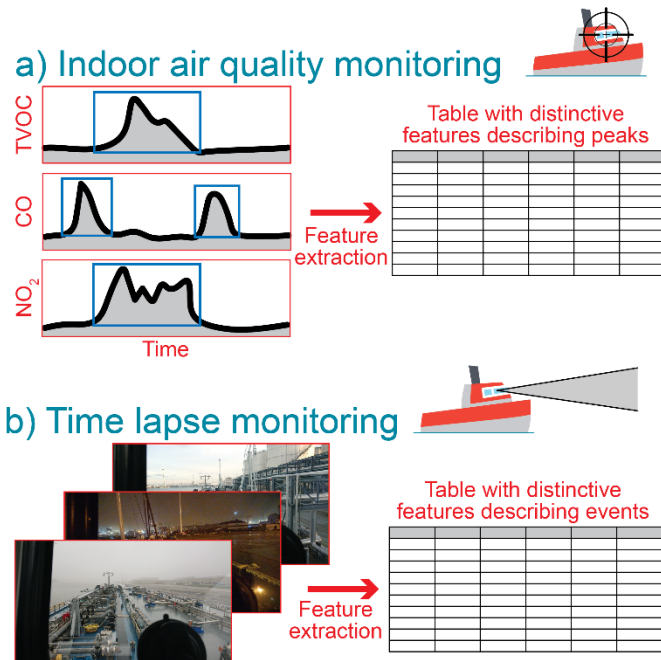


Fig. 2: Visual representation of the methods used to extract distinctive features about events observed in time series and in series of photos.

### 2.3. Data processing of the time-lapse photos

Throughout the day, the time-lapse photos offer a clear view of the ship's environment. At night, artificial illumination often ensures visibility to detect nearby occurrences. Yet, as the ship navigates the Scheldt River during nighttime, the darkness becomes too profound for the camera to capture useful images.

The analysis of the time-lapse imagery is conducted using two distinct methods. The initial technique pinpoints specific instances where notable events occur, such as the ship docking at a quay, waiting inside a lock, encountering close passage with another vessel, experiencing rainfall (evidenced by droplets on the window), or engaging in fuel transactions with merchant ships. By analyzing changes in visual cues or anomalies in the sequence of images, numerous events are identified. Some of the events might coincide. It is noteworthy that the maxima of pollution peaks may not coincide with any identified event or might intersect with several concurrent events.

An alternative method splits the photo series into distinct segments by detecting change points. Change points represent marked alterations in the dynamics of the series [24,25]. Change points used in this study are transitions between movement and stationary phases. In the segmentation approach, every peak or cluster of peaks in the air quality data aligns distinctly within one of the delineated segments.

Although the two methods diverge in their approach, the resultant moments are characterized using a consistent set of attributes. The collated and condensed findings are detailed in a table, incorporating features such as:

- **Timestamp start event:** This timestamp marks the initial moment of a notable occurrence or situation in or around the ship;
- **Timestamp end event:** This timestamp indicates when the salient activity or situation ends;
- **Duration:** Represents the total time measured in minutes from the start to the end of the event. This metric quantifies the length of the period;
- **Status of Ship:** Described by the binary variable 'Sailing' or 'Standing still', indicating the ship's activity;
- **Surroundings:** Categorizes the events into one of the following broad categories: 'Harbour', 'Canal', and 'Open water';
- **Event Description:** Describes the activity identified in the series of photos within the marked event using words.

### 3 RESULTS

Fig. 2 illustrates the dynamic patterns present in the time series of temperature, relative humidity, and CO<sub>2</sub>, displaying their relationship with the ship's position. Within these time series, numerous peaks are observed atop a slowly fluctuating baseline. From the extracted features, the six peaks with the highest z-score have been identified and ranked. These peaks are numbered from highest to lowest significance and shown in Fig. 2. Some moments are characterized by a single and isolated peak with a single maximum (e.g., peak 5), while others display a series of overlapping peaks with multiple local maxima (e.g., peak 3). Peaks exhibiting shoulders are challenging to classify in the binary classification as 'single peaks' or 'series of peaks' because they may consist of several peaks that are hard to resolve. The synchrony between CO<sub>2</sub>, relative humidity (RH), and temperature (T) is indicative of human presence in the wheelhouse. Peak height relative to the baseline is at many occasions highest for CO<sub>2</sub>, followed by relative humidity, while temperature fluctuations are more subtle. During periods of changing ship positions over time (e.g., blue rectangles in Fig. 2), higher CO<sub>2</sub> and RH levels are observed in the wheelhouse, reflecting the presence of the crew required to operate the ship. It should be remarked that warm and humid exhaust gas also contains CO<sub>2</sub> and that this synchrony can be explained differently.

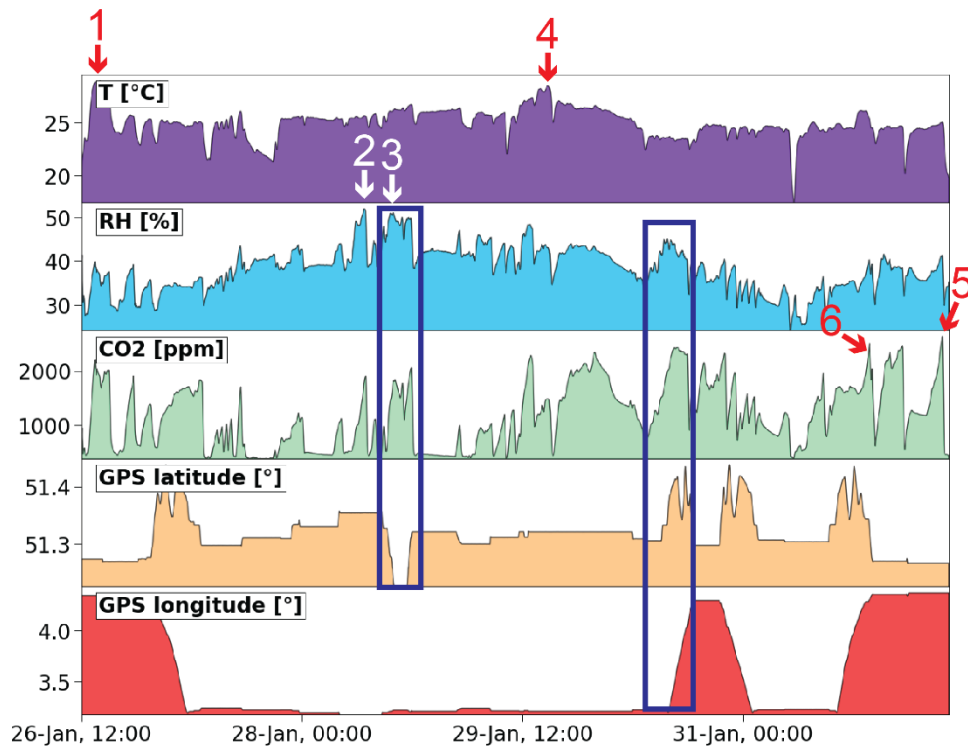


Fig. 2: Temperature, relative humidity and CO<sub>2</sub> measurements in the wheelhouse over time.

A total of 67 peaks in temperature (T), relative humidity (RH), and carbon dioxide (CO<sub>2</sub>) levels have been identified. The six most significant peaks, indicated by their highest z-scores, are illustrated in Fig. 2 and detailed in Table I. Table I shows that it is possible to describe the peaks shown in Fig. 2 with several properties organized in a table. In the time-lapse photos and GPS-data give an insight about the surroundings of the ship. Upon comparing the peak maxima with the segments in which the maximum value falls, it is observed that 6 peaks occur at the beginning of the segment, while 10 occur at the end of the segment. This suggests occasional synchrony between environmental peaks and the change points. The change points used in this study are transitions between the ship moving and the ship standing still. Such transition requires more maneuvers. When considering all kinds of events including the ones occurring in the surroundings of the ship, the peak maxima do not consistently align with periods when events occur, although there may be partial overlap between the periods where peaks and events occur. Consequently, not all peaks could be attributed to an event. The comparison with events did not yield significant additional information.

TABLE I: Description of the 6 most important peaks for T, RH and CO<sub>2</sub> according to the extracted features and the features of the segment in which the peak maximum resides.

Feature	1	2	3	4	5	6
<b>Features from peaks identified in monitoring campaign</b>						
Timestamp start	26/01/'21 12:08	28/01/'21 08:16	28/01/'21 13:05	29/01/'21 14:07	01/02/'21 02:40	31/01/'21 13:52
Timestamp maximum	26/01/'21 15:02	28/01/'21 10:07	28/01/'21 14:26	29/01/'21 16:04	01/02/'21 08:29	31/01/'21 20:36
Timestamp end	26/01/'21 16:41	28/01/'21 10:35	28/01/'21 18:09	29/01/'21 16:25	01/02/'21 08:41	31/01/'21 21:21
Duration [in minutes]	272.95	138.45	303.97	138.45	361.20	448.46
Parameter	T	RH	RH	T	CO <sub>2</sub>	CO <sub>2</sub>
Shape	Series of peaks	Series of peaks	Series of peaks	Single peak	Single peak	Series of peaks
Maximum value	28.97	52.04	51.04	28.49	2636.80	2511.60
Corresponding z-score	2.81	2.71	2.51	2.48	2.42	2.21
GPS latitude	51.27413	51.35521	51.31039	51.32165	51.26689	51.32649
GPS longitude	4.343061	3.176239	3.206757	3.210866	4.371531	4.307178
<b>Features from the corresponding segment as identified with time-lapse photography</b>						
Timestamp start	26/01/'21 11:25	28/01/'21 06:16	28/01/2021 13:50	29/01/2021 13:01	01/02/2021 03:09	31/01/2021 20:23
Timestamp end	26/01/'21 15:13	28/01/'21 12:54	28/01/2021 15:04	30/01/2021 05:48	01/02/2021 09:34	31/01/2021 21:17
Duration [in minutes]	227.9	397.9	74.3	1007.5	385.7	54.2
Time between peak maximum and beginning of segment [in minutes]	216.9	231.8	35.9	183.0	319.9	12.7
Time between end of segment and peak maximum [in minutes]	11.0	166.1	38.3	824.5	65.8	41.5
Status ship	Standing still	Standing still	Sailing	Standing still	Standing still	Sailing
Surroundings	Harbour	Harbour	Canal	Harbour	Harbour	Harbour
Event description	Ship is at the quay in the port of Antwerp	Ship is delivering fuel to a merchant ship in Bruges-on-Sea (it is raining)	Ship sails in the docks of Bruges-on-Sea and there is a bridge in front	Ship is at the quay behind another inland ship in Bruges-on-Sea	Ship is at the quay next to an inland tanker in the port of Antwerp	Ship sails in the docks of the port of Antwerp

Figure 3 demonstrates the variations over time in pollutant concentrations caused by the combustion of fuel in the engine's cylinders when there is a lack of oxygen, caused by a departure from the optimal air-to-fuel ratio. In such scenarios, combustion leads to the formation of partially oxidized carbon, resulting in the emission of CO, TVOC, and PM. It is important to note that TVOC emissions may also originate from the cargo of the inland tanker, which can be released during the periods of bunkering. For this category of pollutants, the 6 most important peaks have been identified using the z-score, ranked according to its importance, and numbered. The numbered peaks are shown in Fig. 3. Besides the 6 most important peaks, the time series contains many more peaks. Instances of combustion with inadequate air supply are observed to occur regularly during the journey, as shown in Figure 3. In total, 91 moments with peaks have been identified. The extracted features also allow for the calculation of the total exposure time of all PM<sub>10</sub> peaks, which accounts for 71% of the total period of the measurement campaign. For PM<sub>1</sub>, PM<sub>2.5</sub>, CO, and TVOC, this exposure time is 58%, 57%, 39%, and 35% respectively. Although the pollution peaks remain below imposed thresholds, the impact of such pollution peaks on human health cannot be neglected. Additionally, the sensor box detects synchronous occurrences of peaks, such as between CO and TVOC (e.g., peak 4 and 5) or between CO, TVOC, and PM (e.g., peak 3 and 6).

While GPS information provides insight into whether the ship is moving or stationary, it does not elucidate why pollution peaks occur. Through segmentation of the journey using time-lapse photography, it is observed that 33% of the peaks fall within segments when the ship is sailing, 31% during bunkering activities, 33% when the ship is waiting at the quay, and 3% during waiting in a lock (see Table II). However, this distribution is not substantially different from that observed for pollutants such as NO, NO<sub>2</sub>, and O<sub>3</sub>.

The widths of the six most important peaks range from 90 minutes (PM<sub>10</sub> peak 2) to 1200 minutes (PM<sub>2.5</sub> peak 1) at the baseline, suggesting that they are unlikely to be caused by passing ships, which typically take less than 5 minutes to pass. The most significant peak, nr. 1, occurs during a bunkering operation, while peak number 2 is observed when the ship is docked at a quay. For the other peaks, the ship is sailing. There appears to be no clear synchrony between the peaks of pollutants and the segments of the journey. This suggests that additional contextual information is required to explain the occurrence of these peaks.

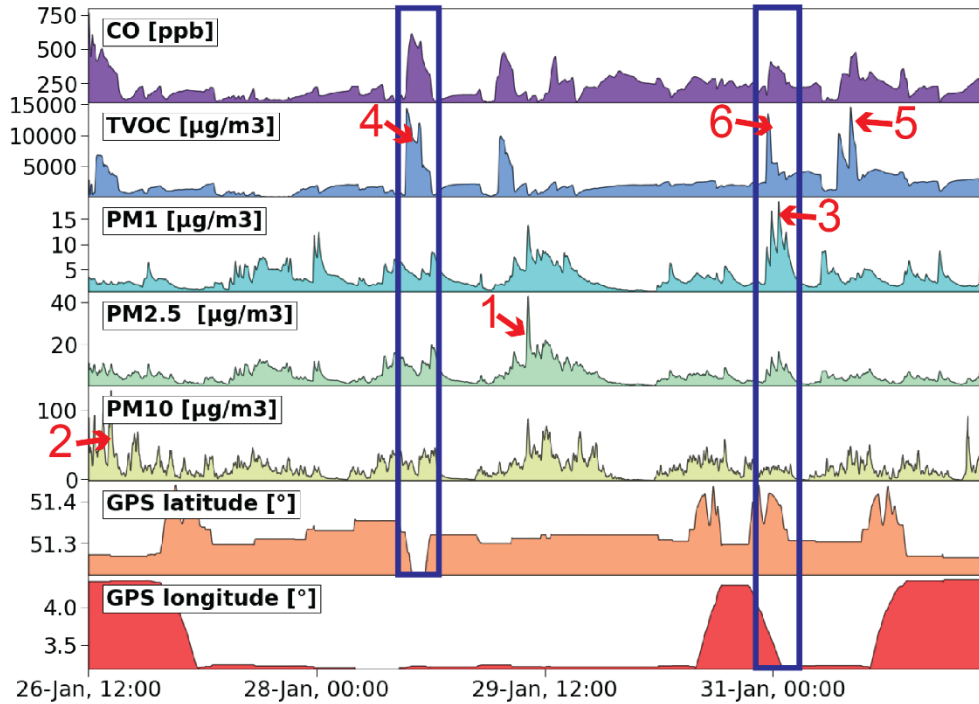


Fig. 3: Time series plots of pollutants formed in a low-oxygen environment and the 6 most important peaks.

Fig. 4 illustrates the time-series dynamics of pollutants generated when fuel is burned in the engine’s cylinders in an excess of oxygen gas. Among the monitored pollutants in this category are NO, NO<sub>2</sub>, and O<sub>3</sub>. These time series encompass 41 moments with peaks. Although these peaks exhibit widths at the baseline ranging from 20 to 1000 minutes, their potential impact on human health cannot be dismissed, as the total exposure of NO<sub>2</sub>, O<sub>3</sub>, and NO peaks constitutes 41%, 33%, and 19% of the total measuring campaign, respectively. However, the exposure times are somewhat lower compared to the pollutants shown in Fig. 3. The blue squares in Fig. 4 indicate the synchrony between NO and NO<sub>2</sub> while the ship is sailing.

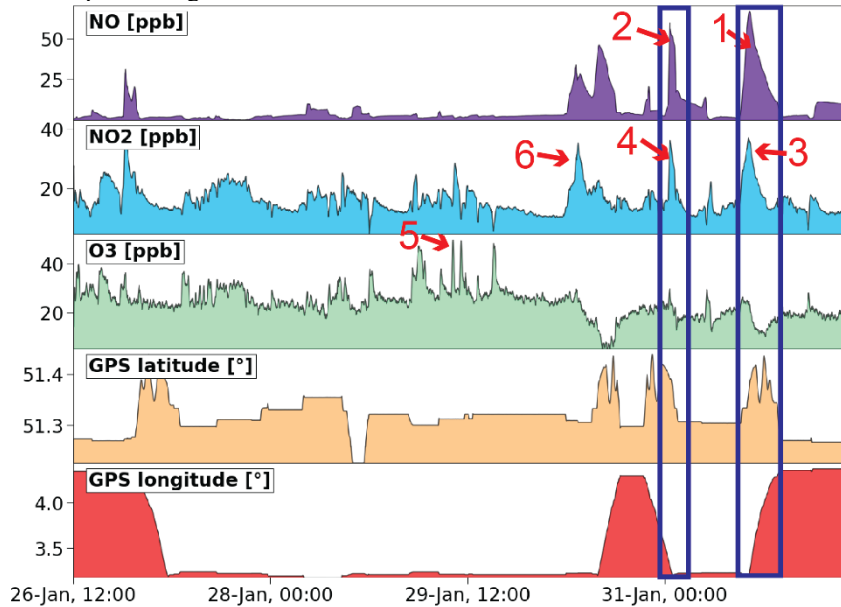


Fig. 4: Time series plots of pollutants formed in an excess of air and the 6 most important peaks.

Table II gives a classification of the NO, NO<sub>2</sub> and O<sub>3</sub> peaks according to the status and activity of the ship. Of all these peaks, 37% corresponds with segments when the ship is sailing, 37% when the ship is bunkering, and 27% when the

ship is waiting at a quay (see Table II). None of the peaks could be associated with a segment where the ship is waiting inside a lock. The same classification has been performed for the CO, TVOC and PM-peaks. Table II does not show an obvious difference between the two categories of pollutants.

TABLE II: Percentage of peaks that can be associated to specific segment types of the journey.

Segment type	NO, NO <sub>2</sub> , O <sub>3</sub> peaks	CO, TVOC, PM peaks
Sailing	37 %	32 %
Bunkering	37%	31 %
Waiting at a quay	27 %	33 %
Waiting in a lock	0 %	3 %
Total number of peaks	41 peaks	91 peaks

Among the six most important peaks for the category of pollutants shown in Fig. 5, the first four occur while sailing close to the shore of the North Sea. The green arrows in Fig. 5 indicate the synchrony between NO and NO<sub>2</sub> peaks. Peak nr. 1 is observed as the ship sails approximately 5 km off the North Sea coast near Bruges-on-Sea. Two merchant ships can be seen on the images at portside at around 15:27 at some distance. Although night images provide limited details, GPS data offers clues to the ship's location. The O<sub>3</sub> peak nr. 5 happens as the ship is alongside another merchant vessel during a fueling operation. The NO<sub>2</sub> peak nr. 6 arises shortly after completing fuel delivery to a merchant ship, as it maneuvers backwards to dock at the quay behind that merchant ship and begins refueling from trucks. Although some peaks are close to the beginning of the segment (i.e.n peak 4), the relationship is not as apparent as for temperature, relative humidity, and CO<sub>2</sub>.

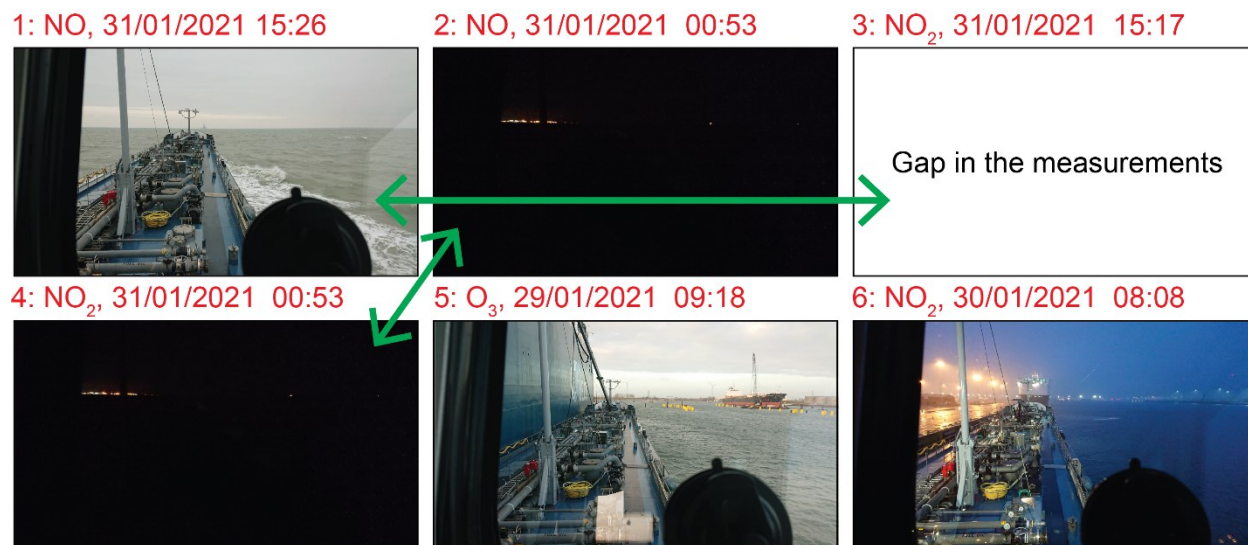


Fig. 5: Time-lapse images corresponding with the moments of the maxima of the 6 peaks.

#### 4 CONCLUSIONS

The examination of dynamic patterns within the time series data revealed a plethora of short-term features, including isolated peaks, series of overlapping peaks, and valleys atop fluctuating baselines. These features, often denoted as outliers, signify sudden deviations in pollutant concentrations and underscore the complex nature of pollution dynamics within the wheelhouses. Further exploration focused on categorizing and understanding the origins of these outliers. It was discerned that peaks in pollutants might arise from various sources, including the ship's own exhaust emissions, passing ships, nearby industrial activities, or specific ship-related operations such as bunkering. Additionally, the analysis unveiled sporadic synchrony between pollution events and change points, suggesting temporary relationships between pollution events and ship activities. Notably, the integration of time-lapse photography provided valuable contextual information, aiding in the identification of events occurring in the vicinity of the ship. By juxtaposing pollutant peaks with these events, insights into potential causative factors have been gained. However, despite these efforts, a clear synchrony between pollutant peaks and journey segments is not evident, indicating the need for further contextual elucidation. In conclusion, this study underscores the multifaceted nature of

pollution dynamics within inland ship wheelhouses and highlights the importance of incorporating diverse data sources and analytical techniques to unravel the complex interplay between environmental factors and ship-related activities. Moving forward, a deeper understanding of these dynamics will be essential for devising effective strategies to mitigate pollution and safeguard the health and well-being of ship crews and the environment.

## REFERENCES

1. Schalm, O.; Carro, G.; Lazarov, B.; Jacobs, W.; Stranger, M. Reliability of lower-cost sensors in the analysis of indoor air quality on board ships. *Atmosphere* [online]. 2022, vol. 13, no. 10, p. 1579. [Accessed: 7 May 2024]. eISSN: 2073-4433. Available at: <https://doi.org/10.3390/atmos13101579>
2. Schalm, O.; Carro, G.; Jacobs, W.; Lazarov, B.; Stranger, M. The inherent instability of environmental parameters governing indoor air quality on board ships and the use of temporal trends to identify pollution sources. *Indoor Air* [online]. 2023, 2023, 1–19. [Accessed: 7 May 2024]. eISSN: 1600-0668. Available at: <https://doi.org/10.1155/2023/7940661>
3. Busch, D.; Krause, K. Air quality on the Rhine and in the Inland Ports of Duisburg and Neuss –. *Immissionsschutz* [online]. Berlin: Erich Schmidt Verlag, May 2021, vol. 2, p. 78-85. [Accessed: 7 May 2024]. Available at: <http://dx.doi.org/10.37307/j.1868-7776.2021.02.05>
4. Eger, P.; Mathes, T.; Zavarsky, A.; Duester, L. Measurement report: inland ship emissions and their contribution to NO<sub>x</sub> and ultrafine particle concentrations at the Rhine. *Atmospheric Chemistry and Physics* [online]. 2023, vol. no. 23, p. 8769–8788. [Accessed: 7 May 2024]. eISSN: 1680-7324. Available at: <https://doi.org/10.5194/acp-23-8769-2023>
5. Huang, H.; Zhou, C.; Huang, L.; Xiao, C.; Wen, Y.; Li, J.; Lu, Z. Inland ship emission inventory and its impact on air quality over the Middle Yangtze River, China. *Science of The Total Environment* [online]. 15 october 2022, vol. 843, p. 156770. [Accessed: 7 May 2024]. eISSN: 1879-1026. Available at: <https://doi.org/10.1016/j.scitotenv.2022.156770>
6. European Commission. Directorate General for Environment. *Guidance document on inland waterway transport and Natura 2000: sustainable inland waterway development and management in the context of the EU Birds and Habitats Directives* [online]. Luxembourg: Publications Office of the European Union, 2018. [Accessed: 7 May 2024]. ISBN: 9789276022312. Available at: <https://op.europa.eu/en/publication-detail/-/publication/6c766acc-8d84-11e9-9369-01aa75ed71a1>
7. Jiang, H.; Peng, D.; Wang, Y.; Fu, M. Comparison of inland ship emission results from a Real-World Test and an AIS-Based Model. *Atmosphere* [online]. 2021, vol. 12, no. 12, p. 1611. [Accessed: 7 May 2024]. eISSN: 2073-4433. Available at: <https://doi.org/10.3390/atmos12121611>
8. Pillot, D.; Guiot, B.; Cottier, P.L.; Perret, P.; Tassel, P. Exhaust emissions from in-service inland waterways vessels. *Journal of Earth Sciences and Geotechnical Engineering* [online]. 2016, vol. 6, no. 4, p. 205–225. [Accessed: 7 May 2024]. eISSN: 1792-9660. Available at: <http://www.scienpress.com/download.asp?ID=1931>
9. Zhang, X.; Van Der A, R.; Ding, J.; Zhang, X.; Yin, Y. *The impact of inland ship emissions on air quality* [online]. EGU sphere preprint, 2022. [Accessed: 7 May 2024]. Available at: <https://doi.org/10.5194/egusphere-2022-1411>
10. Webster, A.D.; Reynolds, G.L. Indoor Air Quality on Passenger Ships. In: Hocking, M. (ed). *Air quality in airplane cabins and similar enclosed spaces* [online]. Berlin/Heidelberg: Springer, 2005. The Handbook of Environmental Chemistry, vol. 4H, p. 335–349. ISBN 978-3-540-25019-7, eISBN: 978-3-540-31491-2. [Accessed: 7 May 2024]. Available at: <https://doi.org/10.1007/b107251>
11. Carro, G.; Jacobs, W.; Storme, P.; Cabal, A.; Demeyer, S.; Schalm, O. A new approach to make indoor air quality in the accommodation of ships understandable and actionable for seafaring staff. In: *International Conference on Maritime Transport. 8th International Conference on Maritime Transport (Maritime Transport VIII): Barcelona, 17-18 September* [online]. Barcelona: Universitat Politècnica de Catalunya. Departament de Ciència i Enginyeria Nàutiques, 2020; p. 18. [Accessed: 7 May 2024]. ISBN: 9788498808278. Available at: <http://hdl.handle.net/2117/330014>
12. Liu, Z.; Lu, X.; Feng, J.; Fan, Q.; Zhang, Y.; Yang, X. Influence of ship emissions on urban air quality: a comprehensive study using highly time-resolved online measurements and numerical simulation in Shanghai. *Environmental Science & Technology* [online]. 2017, vol. 51, no. 1, p. 202–211. [Accessed: 7 May 2024]. Available at: <https://doi.org/10.1021/acs.est.6b03834>
13. Sorte, S.; Rodrigues, V.; Borrego, C.; Monteiro, A. Impact of harbour activities on local air quality: a review. *Environmental Pollution* [online]. February 2020, vol. 257, p. 113542. [Accessed: 7 May 2024]. eISSN: 1873-6424. Available at: <https://doi.org/10.1016/j.envpol.2019.113542>

14. Ledoux, F.; Roche, C.; Cazier, F.; Beaugard, C.; Courcot, D. Influence of ship emissions on NO<sub>x</sub>, SO<sub>2</sub>, O<sub>3</sub> and PM concentrations in a North-Sea harbor in France. *Journal of Environmental Sciences* [online]. September 2018, vol. 71, p. 56–66. [Accessed: 7 May 2024]. eISSN: 1878-7320. Available at: <https://doi.org/10.1016/j.jes.2018.03.030>
15. Mueller, D.; Uibel, S.; Takemura, M.; Klingelhofer, D.; Groneberg, D.A. Ships, ports and particulate air pollution - an analysis of recent studies. *Journal of Occupational Medicine Toxicology* [online]. 2011, vol. 6, no. 31. [Accessed: 7 May 2024]. eISSN: 1745-6673. Available at: <https://doi.org/10.1186/1745-6673-6-31>
16. Wang, X.; Shen, Y.; Lin, Y.; Pan, J.; Zhang, Y.; Louie, P.K.K.; Li, M.; Fu, Q. Atmospheric Pollution from Ships and Its Impact on Local Air Quality at a Port Site in Shanghai. *Atmospheric Chemistry and Physics* [online]. 2019, vol. 19, no. 9, 6315–6330. [Accessed: 7 May 2024]. eISSN: 1680-7324. Available at: <https://doi.org/10.5194/acp-19-6315-2019>
17. Tallon-Ballesteros, A.J.; Riquelme, J.C. Deleting or keeping outliers for classifier training? In: *2014 Sixth World Congress on Nature and Biologically Inspired Computing (NaBIC 2014), Porto, Portugal, July 2014*, [online]. IEEE, 2014, p. 281-286. [Accessed: 7 May 2024]. Available at: <https://doi.org/10.1109/NaBIC.2014.6921892>
18. Chandola, V. Anomaly detection : a survey. *ACM Computing Surveys* 2009, vol. 41, no. 3, p. 1–58. [Accessed: 7 May 2024]. eISSN: 1557-7341. Available at: <https://doi.org/10.1145/1541880.1541882>
19. Olteanu, M.; Rossi, F.; Yger, F. Challenges in anomaly and change point detection. In: *ESANN. proceedings, European Symposium on Artificial Neural Networks, Computational Intelligence and Machine Learning. Bruges (Belgium) and online event, 5-7 October 2022* [online]. Bruges, October 2022; p. 277–286. [Accessed: 7 May 2024]. Available at: <https://doi.org/10.14428/esann/2022.ES2022-6>
20. González Rivero, R.A.; Morera Hernández, L.E.; Schalm, O.; Hernández Rodríguez, E.; Alejo Sánchez, D.; Morales Pérez, M.C.; Nuñez Caraballo, V.; Jacobs, W.; Martínez Laguardia, A. A low-cost calibration method for temperature, relative humidity, and carbon dioxide sensors used in air quality monitoring systems. *Atmosphere* [online]. 2023, vol. 14, no. 2, p. 191. [Accessed: 7 May 2024]. eISSN: 2073-4433. Available at: <https://doi.org/10.3390/atmos14020191>
21. Hernández-Rodríguez, E.; González-Rivero, R.A.; Schalm, O.; Martínez, A.; Hernández, L.; Alejo-Sánchez, D.; Janssens, T.; Jacobs, W. Reliability testing of a low-cost, multi-purpose arduino-based data logger deployed in several applications such as outdoor air quality, human activity, motion, and exhaust gas monitoring. *Sensors* [online]. 2023, vol. 23, no. 17, p. 7412. [Accessed: 7 May 2024]. eISSN: 1424-8220. Available at: <https://doi.org/10.3390/s23177412>
22. González Rivero, R.A.; Schalm, O.; Alvarez Cruz, A.; Hernández Rodríguez, E.; Morales Pérez, M.C.; Alejo Sánchez, D.; Martínez Laguardia, A.; Jacobs, W.; Hernández Santana, L. Relevance and reliability of outdoor SO<sub>2</sub> monitoring in low-income countries using low-cost sensors. *Atmosphere* [online]. 2023, vol. 14, no. 6, p. 912. [Accessed: 7 May 2024]. eISSN: 2073-4433. Available at: <https://doi.org/10.3390/atmos14060912>
23. Sebestyen, G.; Hangan, A.; Kovacs, G. Platform for anomaly detection in time-series. In: *XXXIV Kandó Konferencia* [online]. 2018, p. 14-26. [Accessed: 7 May 2024]. Available at: <http://kttk.kvk.uni-obuda.hu/sites/default/files/csatoImany/sip2018-papers-en-v2.pdf>
24. Dalheim, Ø.Ø.; Steen, S. A computationally efficient method for identification of steady state in time series data from ship monitoring. *Journal of Ocean Engineering and Science* [online]. December 2020, vol. 5, no. 4, p. 333–345. [Accessed: 7 May 2024]. eISSN: 2468-0133. Available at: <https://doi.org/10.1016/j.joes.2020.01.003>
25. Guralnik, V.; Srivastava, J. Event detection from time series data. In: *KDD'00 : Proceedings of the fifth ACM SIGKDD International Conference on Knowledge Discovery and Data Mining*. New York: ACM Press, 1999; p. 33–42. ISBN: 9781581131437.